Optical characterization of $2k_F$ bond-charge-density wave in quasi-one-dimensional $\frac{3}{4}$-filled $(EDO\text{-}TTF)_2X$ ($X=PF_6$ and AsF_6)

Olga Drozdova,[1,2,3,*] Kyuya Yakushi,[1] Kaoru Yamamoto,[1] Akira Ota,[2] Hideki Yamochi,[2] Gunzi Saito,[2] Hidenori Tashiro,[3] and David B. Tanner[3]

[1]*Institute for Molecular Science, Okazaki Aichi 444-8585, Japan*

[2]*Division of Chemistry, Graduate School of Science, Kyoto University, Sakyo-ku Kyoto 606-8502, Japan*

[3]*Department of Physics, University of Florida, Gainesville Florida 32611-8440, USA*

(Received 14 October 2003; revised manuscript received 9 February 2004; published 23 August 2004)

We present the electronic and vibrational spectra of quasi-one-dimensional $\frac{3}{4}$-filled $(EDO\text{-}TTF)_2X$ (EDO-TTF=ethylenedioxy-tetrathiafulvalene, $X=PF_6$ and AsF_6) above and below the metal-insulator phase transition ($T_{MI}=280$ K for the PF_6 salt and 268 K for the AsF_6 salt). For the low-temperature insulating phase, the pattern of both bond and charge order was identified. Almost all charge density is localized on the strongly bound central pair of 0110 tetramer giving rise to a characteristic spectrum of electronic excitations. Infrared spectra along the stacking axis show evidence of strong electron-molecular vibration coupling between the charge transfer band within the pair and some specific intramolecular vibrations. This charge order is assisted by a molecular deformation.

DOI: 10.1103/PhysRevB.70.075107 PACS number(s): 71.30.+h, 71.45.Lr, 78.30.−j, 71.27.+a

I. INTRODUCTION

Ground states of strongly correlated electron systems involving inhomogeneous site-charge distribution, or charge ordering (CO), have received recently much interest in both experiment and theory.[1,2] Organic charge-transfer solids (CTS) are an important class of materials exhibiting CO owing to a variety of CO states, a chance of coexistence with a commensurate bond order wave (BOW) and spin density wave,[3] tunability of a CO pattern by a small chemical modification of the crystal parameters,[4] and proximity on the phase diagram and likely the similar driving forces leading to CO as well as to a superconducting state.[5] In quasi-one-dimensional (Q1D) $\frac{3}{4}$- or $\frac{1}{4}$-filled organic CTS, a large on-site (U) and nearest-neighbor (V) Coulomb repulsion would cause, intuitively, the alternating (Wigner type) pattern of charge distribution 1010 (where 0 and 1 sites have charge densities of $(0.5-\delta)$ and $(0.5+\delta)$ electron charge, respectively) corresponding to a $4k_F$ charge density wave (CDW). A number of theoretical studies have argued that such a periodicity requires V exceeding some critical $V_c \sim 2t$ (t is the intrastack transfer integral).[6] On the other hand, for $V<V_c$, the 0110 ground state can be found.[7] This state corresponds to a $2k_F$ CDW coupled with BOW of SW′SW type (the strongest bond S connects 1 and 0 sites, and W' and $W(<W')$ exist in pairs 11 and 00, respectively) [Fig. 1(a)], which we call below as $2k_F$ BCDW-I. From numerical calculations, it is expected to have a small site-charge difference 2δ and a large BOW.[7] Such $2k_F$ BCDW-I was found, for example, in $D_2(TCNQ)$ salts, where D=MEM, TEA tetracyanoquinodimethane (TCNQ); *N*-methyl-*N*-ethyl-morpholinium (MEM); tetraethylammonium (TEA).[7] When V is further small, 0110 CO can coexist with a different BOW of $W'SW'W$ sequence Fig. 1(b) called below as $2k_F$ BCDW-II,[8] which has not previously been definitely confirmed in any organic CTS.

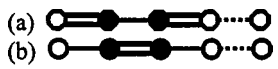

FIG. 1. $2k_F$ BCDW-I (a) and $2k_F$ BCDW-II (b).

Recently, Q1D organic CTS $(EDO\text{-}TTF)_2X$ (where EDO-TTF=ethylenedioxy-tetrathiafulvalene and $X=PF_6$ and AsF_6) have been synthesized.[9] A first order metal-insulator (MI) phase transition was observed at $T_{MI}=280$ K in the PF_6 salt and 268 K in the AsF_6 salt. The mechanism of the MI transition did not conform to any particular kind of the phase instability found in organic CTS before, and was proposed as a type complying with the simultaneous cooperation of the Peierls, CO, and anion order features.[9] From the x-ray crystal structure analysis, it was determined that the unit cell is doubled. A distinctive deformation of EDO-TTF was found in the low-temperature insulating phase. The molecular bond lengths suggest an "0110" CDW and the calculation of the overlap integrals gives a $W'SW'W$ type of BOW. Our preliminary optical study of the PF_6 salt[10] has established two types of molecular charges ($<+0.1$ and $>+0.9$), and two charge-transfer (CT) bands, consistent with a $2k_F$ BCDW-II. In this paper, we present the full electronic and vibrational spectra and their analysis for both salts with the aim to give a complete optical characterization of the structure and interactions in the rare $2k_F$ BCDW-II state.

II. EXPERIMENT

Single crystals grown by an electrocrystallization technique were black lustrous plates of $1.0\times0.3\times0.05$ mm^3 dimensions.[9] The most developed crystal face was (001) elongated along the b axis. The polarized reflectivity data were measured with two spectrometers, Fourier transform infrared Nicolet Magna 760 ($600-12\,000$ cm^{-1}), and multichannel detection system Atago Macs 320 ($11\,000-33\,000$ cm^{-1}), both combined with infrared (IR)

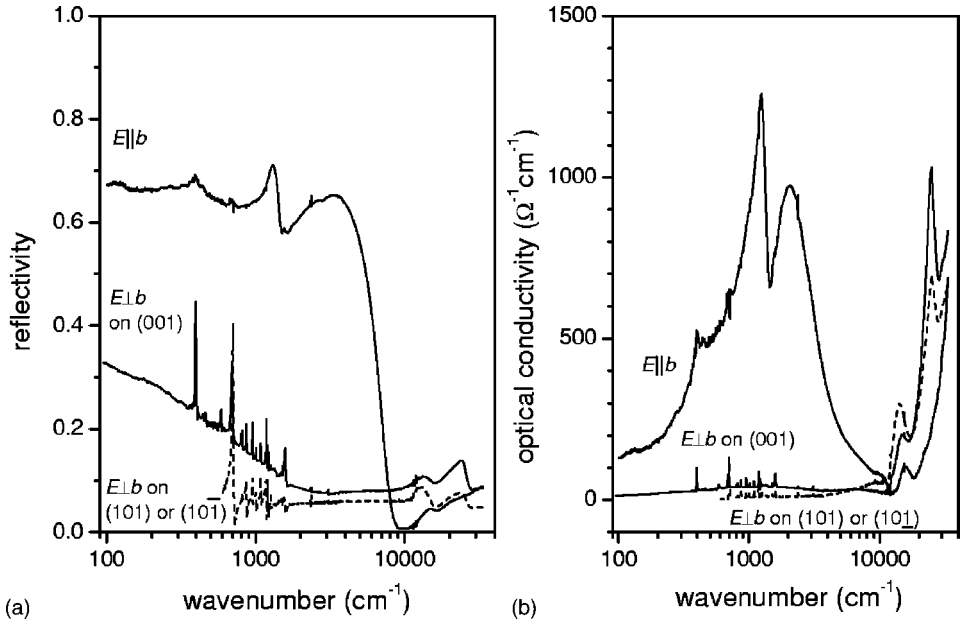

FIG. 2. (a) Polarized reflectivity and (b) optical conductivity spectra of $(EDO\text{-}TTF)_2AsF_6$ at 300 K.

microscope. Temperature dependence was obtained at slow sample cooling (2–6 K/h) using Oxford CF1104s cryostat. The sample was first heated up to 310 K and then the spectra were taken at 310, 290, 270, 250, 200, 100, and 6 K for PF_6 salt and at 300, 270, 260, 200, 100, and 6 K for AsF_6 salt. The far-IR polarized reflectivity (90–700 cm^{-1}) at room temperature (RT) was measured on the single crystal of the AsF_6 salt using Bruker IFS-113v spectrometer. Polarized Raman spectra were measured in 180° backreflecting geometry with Renishaw Ramascope System-1000 equipped with three lasers: Ar^+ ($\lambda=515$ nm), He-Ne ($\lambda=633$ nm), and near-infrared laser diode (LD) ($\lambda=785$ nm). Spectra were taken at 300, 200, and 4.2 K at slow cooling using the above cryostat system. The isostructural PF_6 and AsF_6 salts were found to give almost identical spectra between them while in the same electronic state. Therefore, later in the figures we show the spectra mostly for the AsF_6 salt and include numerical values for both where appropriate.

III. RESULTS AND DISCUSSION

A. High-temperature phase

1. Electronic spectra

The room-temperature crystal structure is isomorphous to that of the Bechgaard salts, where two donor molecules connected by an inversion center are stacked along the b axis (weak $4k_F$ BOW) and form a conducting sheet in the (001) plane.[9] The conducting sheets are separated by anion layers. Reflectance spectra of the AsF_6 salt at RT for three main crystal directions are shown in Fig. 2(a). Along the stacking axis ($E\|b$) the Drude-like feature is prevalent. Although the absolute reflectivity in the low frequency region is high ($\sim$0.70 for PF_6 salt and 0.65 for AsF_6 salt), it does not raise significantly in the far-IR. The spectrum for $E\perp b$ on (001) is reminiscent of an overdamped plasmon and suggests some weak interstack interaction. The anisotropy of the reflectivity in the conducting plane resembles that of Bechgaard salts.[11] The spectrum for the third direction is dominated by the intramolecular vibrations on a low flat background. The optical conductivity spectra were obtained after the Kramers-Kronig analysis of the data from Fig. 2(a), where the low frequency region was extrapolated using the Hagens-Ruben formula for the spectra above T_{MI}, and a constant reflectivity was assumed below T_{MI}. The result is shown on Fig. 2(b). Along the stack, the conductivity exhibits a broad asymmetric peak in the midinfrared region with the spectral weight extending over 10 000 cm^{-1}, which is characteristic of a strongly correlated metal. The peak shape is distorted as well by an electron-molecular vibration (e-mv) resonance near 1340 cm^{-1}, which is consistent with the slightly dimerized structure of the stack. Extrapolating the low-frequency side to $\omega=0$ gives $\sigma_0=50\pm10\ \Omega^{-1}\ cm^{-1}$, which is in good agreement with $\sigma_{dc}=60\ \Omega^{-1}\ cm^{-1}$.[9] Two broad electronic peaks at 16 and 20×10^3 cm^{-1} for PF_6, and 15 and 24×10^3 cm^{-1} for AsF_6 salt were identified as the intramolecular $\pi\rightarrow\pi^*$ transitions of $EDO\text{-}TTF^{+1}$ (later called as LE_1) and $EDO\text{-}TTF^0$ (LE_2), respectively.

2. Vibrational spectra

In organic molecules built on TTF skeleton, the frequencies of the C=C stretching modes are sufficiently sensitive to the molecular charge to allow them to be used for an accurate quantitative estimation of this charge. EDO-TTF has three C=C bonds, all of which become longer as the molecule acquires positive charge. In the descending order of frequencies we call them υ_i^ρ, where $i=\alpha$, β, and γ denote stretching of C=C bonds in the EDO-ring, the TTF-ring, and the bridge, respectively, and ρ shows the molecular (site) charge. The modes were assigned based on the reported data of bis(ethylenedithio)-TTF (BEDT-TTF),[12] bis(ethylenedioxy)-TTF (BEDO-TTF),[13] and ethylenedioxyethylenedithio-TTF (EDOEDT-TTF).[14] Figure 3 shows υ_i^ρ in the Raman spectra of the AsF_6 salt at room

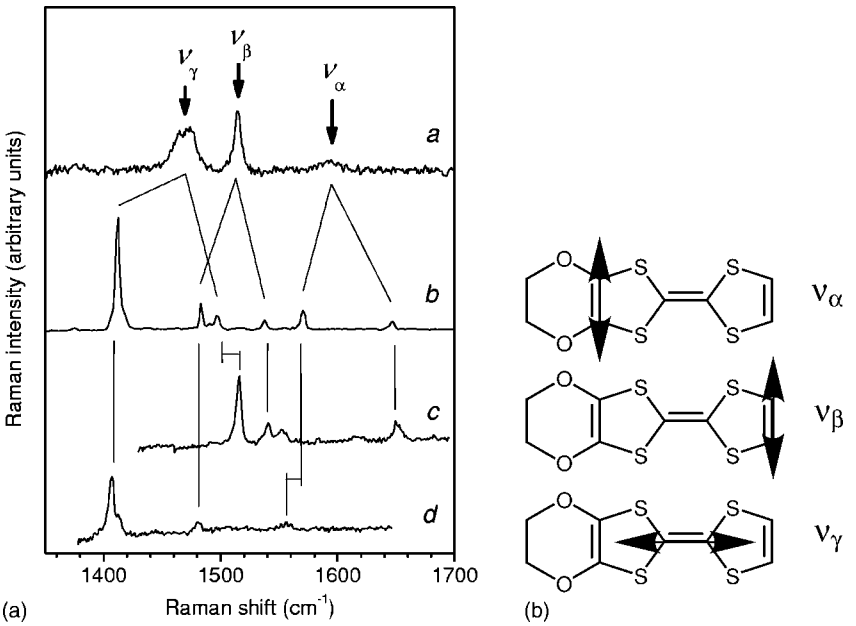

FIG. 3. C═C stretching modes v_i^ρ of EDO-TTF in the Raman spectra of (a) $(EDO\text{-}TTF)_2AsF_6$ at 300 K; (b) $(EDO\text{-}TTF)_2AsF_6$ at 6 K; (c) neutral EDO-TTF; and (d) $(EDO\text{-}TTF)^+IBr_2^-$.

temperature together with the reference spectra for $\rho=0$[15] and +1. The observed frequencies of v_i^ρ are summarized in Table I. In the high-temperature phase a single peak for every mode was observed, and the site charges were estimated as (homogeneous) +0.5. However, the linewidths of v_i^ρ appear to be broadened, although the two sites in the unit cell are crystallographically equivalent to each other. The linewidths of v^α and v^γ are significantly broader than that of v^β. The larger will be the mode splitting below T_{MI}, the broader is the linewidth above T_{MI}. This relation suggests that the line broadening is originated from the dynamical fluctuation of the site-charge density due to the correlation effect. We have simulated the linewidth based on the motional narrowing model taking two equivalent sites and hopping frequency in to account.[16] This simulation reproduced the linewidth of each band shown in Fig. 3(a) (for v^γ, v^β, and v^α, respectively, the experimental linewidth, 21, 7, and 22 cm^{-1}; the simulated linewidth, 16, 8, and 16 cm^{-1}) using the same hopping energy of about 8 meV. This value is interpreted roughly as the hopping energy of the coherently or diffusively moving charge carrier. It should be noted that this hopping energy is more than one order of magnitude small compared with the transfer integrals, which is estimated from the low-temperature electronic spectrum in the next section. From the theoretical point of view, the optical conductivity of strongly correlated system consists of a Drude term and incoherent term.[17] The Drude weight depends upon the effective hopping energy of current carrier.[18] The small hopping energy of the charge carrier is consistent with the observation that the spectral weight of the incoherent part is dominant in the conductivity spectrum.

TABLE I. C═C stretching frequencies of EDO-TTF.

	v_α (cm^{-1})	v_β (cm^{-1})	v_γ (cm^{-1})	Site charge	Symmetry
EDO-TTF	1650	1538	1510	0	(R)
	1654		1515		(IR)
$(EDO\text{-}TTF)IBr_2$	1560	1480	1408	+1	(R)
	1540	1475	1370		(IR)
$(EDO\text{-}TTF)_2PF_6$ at RT	~1592	1515	1472	+0.5	A_g
	1579	1512	~1344		$A_u\,(E\|a)$
$(EDO\text{-}TTF)_2PF_6$ at 6 K	1649	1539	1499	+0.04	A_g
	1648	1539	1496		A_u
	1572	1484	1412	+0.96	A_g
	1564		1383		A_u
$(EDO\text{-}TTF)_2AsF_6$ at RT	~1593	1515	1469	+0.5	A_g
$(EDO\text{-}TTF)_2AsF_6$ at 6 K	1647	1538	1497	+0.04	A_g
	1647	1538	1495		A_u
	1570	1483	1412	+0.96	A_g
	1563		1382		A_u

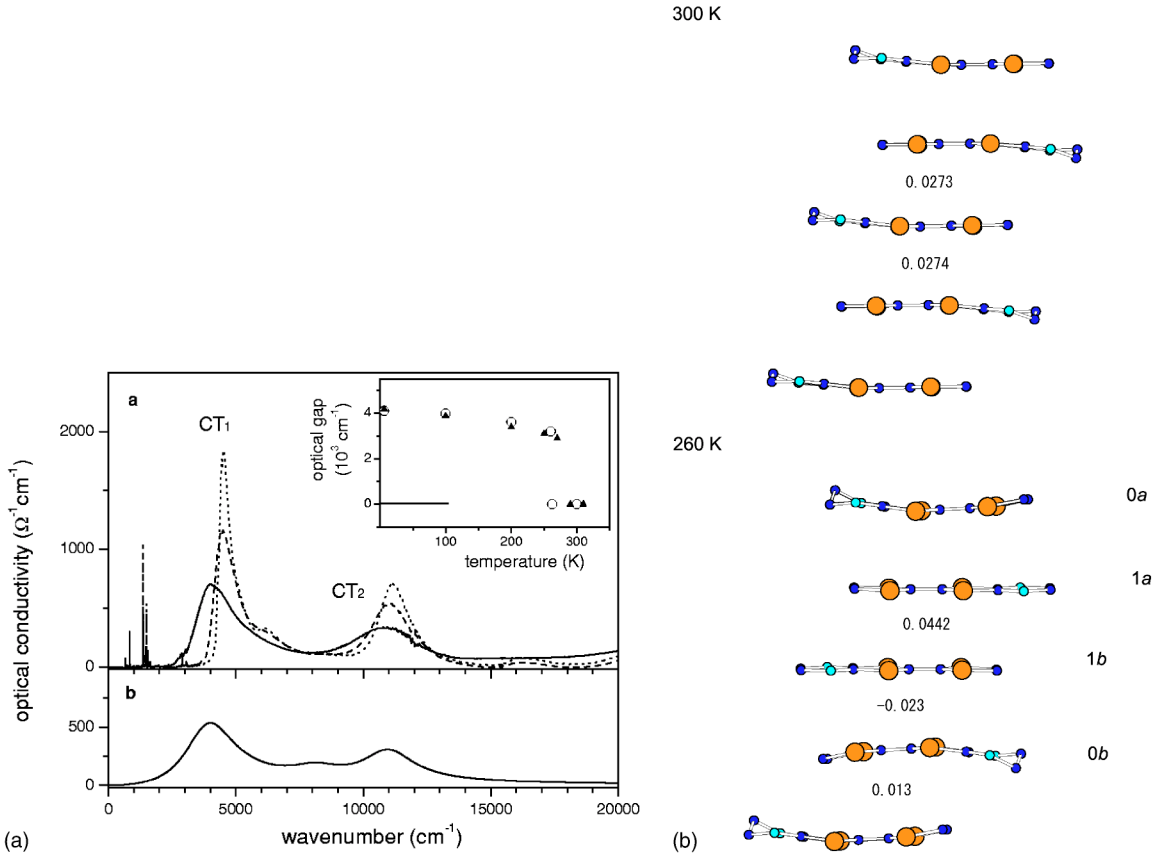

FIG. 4. (a) Stacking-axis optical conductivity spectra of $(EDO\text{-}TTF)_2AsF_6$ at 260 K (solid line), 100 K (dashed line), and 6 K (dotted line); (b) calculated spectrum (see text). The inset shows the temperature dependence of the optical gap (solid triangles and open circles are for PF_6 and AsF_6 salts, respectively). The stacking patterns and the overlap integrals for the PF_6 salt above (top) and below (bottom) T_{MI} are given at the right margin.

B. Low-temperature phase

1. Electronic spectra

As shown in Fig. 4, the low-temperature stack of EDO-TTF forms a tetramer with a small intertetramer overlap integral.[9] The stacking-axis optical conductivity below the phase transition is given in Fig. 4. The broad conductivity peak characteristic of the high-temperature phase [Fig. 2(b)] vanishes abruptly below T_{MI} replaced by two rather sharp electronic peaks at 4500 (CT_1) and 11 150 cm^{-1} (CT_2), which further sharpen and blueshift at lower temperatures. This drastic spectral change indicates the opening of a wide charge gap below T_{MI}, replacing an incoherent feature that exists above T_{MI}. CT_1 is the lowest electronic excitation in the insulating phase. Temperature dependence of the optical gap E_g determined from a linear extrapolation of the leading edge of CT_1 is shown on the inset in Fig. 4. At 6 K $E_g = 0.52$ eV (PF_6) and 0.51 eV (AsF_6) which is two times lower than the one found from the resistivity measurement (activation energy $E_A = 0.52$ eV).[9] Such a difference between the optical and electrical gap is sometimes found for organic semiconductors and should be addressed to a proper theoretical evaluation.

The spectral weight of a particular electronic excitation can be obtained using a partial sum rule

$$\frac{m}{m^*}N_{\text{eff}}(\omega) = \frac{m}{32\pi N_c e^2}\int_0^{\omega}\sigma(\omega')d\omega', \tag{1}$$

where m^* is the effective mass of the carriers, m is a free electron mass, N_c is the carrier density, $N_{\text{eff}}(\omega)$ is the effective number of the charge carriers taking part in the optical transitions in $(0,\omega)$ frequency range, $\sigma(\omega)$ is the optical conductivity, and the upper frequency limit ω is chosen as to cover the region of the charge-transfer bands and avoid a contribution from LE_1 and others above. $(m/m^*)N_{\text{eff}}(\omega)$ is plotted in Fig. 5. At high temperature, the curve rises rapidly at low frequencies and saturates in the visible region to ca. 0.85 $(AsF_6$ salt) and 0.80 $(PF_6$ salt). Below T_{MI}, the total spectral weight does not change, while two distinct plateaus appear associated with the CT bands. The plateaus provide estimations for the oscillator strength $(m/m^*)N_{\text{eff}}(\omega) = 0.50(CT_1) + 0.35(CT_2)$ for AsF_6 salt, and $0.48(CT_1) + 0.32(CT_2)$ for PF_6 salt.

In order to properly assign CT_1 and CT_2, we analyzed the electronic spectrum of $(EDO\text{-}TTF)_2PF_6$ using a Hubbard model for a symmetric tetramer.[19] The sites in the model are denoted as $0a, 1a, 1b$, and $0b$ (see Fig. 4, right margin), and the parameters are t, t_1, Δ, and U (where t and t_1 are the transfer integrals between the sites $0a$ and $1a$ and between

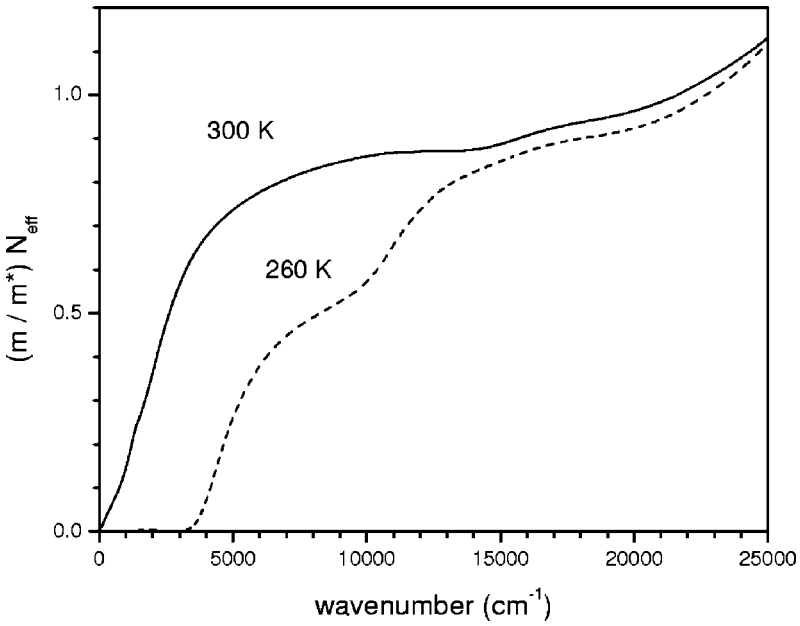

FIG. 5. The sum rule calculation for the $(EDO\text{-}TTF)_2AsF_6$ along the stacking axis at 300 K (solid line) and 260 K (dashed line).

the sites $1a$ and $1b$, Δ and $-\Delta$ are the site energies at the sites $0a$ and $1a$, respectively). Although the model describes an isolated tetramer rather than an infinite tetramerized chain, we assume that, on condition of a small intertetramer overlap integral ($0b$-$0a$), it can reproduce reasonably the general character of the electronic excitations. We searched for the optimal parameters to reproduce the excitation energies, oscillator strengths given earlier, and site charges (0.04 and 0.96), which will be given in the next section. The conductivity spectrum calculated using the optimal parameters ($t=0.15, t_1=0.28, \Delta=0.24, U=0.93$ eV) is drawn in Fig. 4(b). In this model, the singlet ground state consists of the electronic configurations of $|0110\rangle$ (70%), $|0200\rangle$ (16%), and $|1010\rangle$ (9%) with the site-charge difference of 0.86. There are four optically allowed singlet excited states. The first, second, and third excited states respectively involve $|1100\rangle$ (55%) and $|1010\rangle$ (41%); $|1010\rangle$ (55%), $|1100\rangle$ (26%), and $|0200\rangle$ (18%); $|0200\rangle$ (78%), and $|1100\rangle$ (16%). The excitation energies of CT_1 and CT_2 are therefore assigned to the electronic transitions to the first and third excited states, respectively. The spectral weight between 0 and 10 000 cm^{-1} is interpreted as the sum of the transitions to the first and second excited states, and that between 10 000 and 15 000 cm^{-1} as the transition to the third excited state. It should be noted that in order to find a notable intensity of CT_2 in the presence of (main) CT_1, normally, the band filling should be away from $\frac{1}{4}(\frac{3}{4})$ and closer to $\frac{1}{2}$.[20] The fact that CT_2 holds about 40% of the total spectral weight in the nominally $\frac{3}{4}$-filled $(EDO\text{-}TTF)_2X$ ($X=PF_6$ and AsF_6) is unique to this family and can be explained by a cooperation of the large site-charge difference and the type of BOW where the largest transfer integral connects two charge-rich sites. Therefore, this distribution of the spectral intensity can be regarded as a characteristic of the $2k_F$ BCDW-II as opposed to the $2k_F$ BCDW-I or various $4k_F$ states. It was confirmed as well by our numerical calculation. The deformation of the molecule plays the most important role to stabilize the $2k_F$ BCDW-II. As shown in Fig. 4, the deformation of the molecule not only generates the site energy difference, but also enhances the overlap integral between the flat charge-rich molecules. This enhancement contributes to increase the kinetic energy gain between the charge-rich molecules, in other words, decrease $V/2t_1$.

2. Vibrational spectra

Each charge-sensitive band of the high-temperature phase [Fig. 2, curve (a)] splits into two bands below T_{MI} [curve (b)]. The data in Fig. 3 agree entirely with the factor group analysis. Above T_{MI}, six v_i^ρ modes of two $EDO\text{-}TTF^{+0.5}$ are split into $(3A_g+3A_u; A_g$: Raman active, A_u: infrared active). Below T_{MI}, 12 C=C modes are split into $(3A_g+3A_u)$ of the charge-rich molecules, and $(3A_g+3A_u)$ of the charge-poor ones.[21] As will be shown later from the calculation of the vibronic modes in a symmetric tetramer, the least perturbed modes are A_g ones. Using the splitting between the charge-poor and charge-rich A_g branches and taking the weighted average of all three (v_i^ρ) modes, we estimate the site charges below T_{MI} as $\rho=+0.04$ on 0 site, and $\rho=+0.96$ on 1 site (± 0.04).

Intensities of the A_g modes of 0 and 1 site could be enhanced separately using different excitation wavelengths. Figure 6 shows three Raman spectra taken with different lasers, where the excitation wave number of the corresponding laser in relation to the absorption spectra of $EDO\text{-}TTF^0$ and $EDO\text{-}TTF^{+1}$ is given in the inset. The frequency of the Ar^+ laser [curve (a)] is in the region of both LE_2 ($EDO\text{-}TTF^0$) and the second $\pi\rightarrow\pi^*$ transition $EDO\text{-}TTF^{+1}$, so the vibrations of both 0 and 1 sites are enhanced. The frequency of the He-Ne laser is resonant with LE_1 and the corresponding spectrum [curve (b)] shows mainly the modes of the site 1. Because the (intramolecular) $\pi\rightarrow\pi^*$ transitions are polarized in the molecular plane, this is also the direction of the largest Raman intensity in the earlier cases. In contrast, the frequency of the LD laser [curve (c)] is far from any intramolecular electronic transition but close to the (intermolecular) CT_2 energy. This produces a resonance effect with an

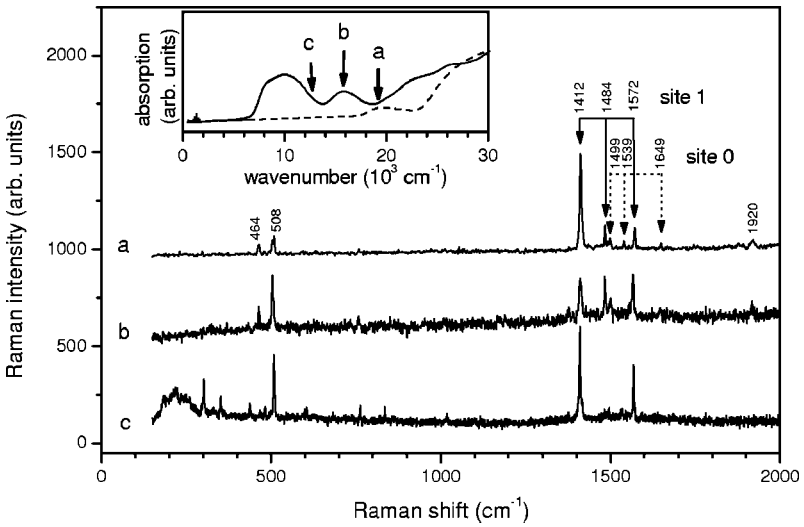

FIG. 6. Raman spectra of $(EDO\text{-}TTF)_2AsF_6$ at 6 K taken with different excitation wavelengths, which are pointed out in the inset with respect to the absorption spectra of $(EDO\text{-}TTF)^+IBr_2^-$ (solid line) and neutral EDO-TTF (dashed line). (a) Ar^+ laser, $E\perp$ stack; (b) He-Ne laser, $E\perp$ stack; (c) LD laser, $E\|$stack.

unusual polarization dependence. While the spectrum polarized in the molecular plane is very weak (not shown), when the polarization is changed to the molecular stack one can observe a strong enhancement of the intensity of some selected modes, among them $v_\alpha^{+0.96}$ ($\sim$10 times as compared to the in-plane polarization under the same experimental conditions) and $v_\gamma^{+0.96}$ ($\sim$50 times). At the same time, the frequencies are not perturbed.

Next, let us examine the e-mv coupling in the IR spectra (A_u modes). Below T_{MI} the stacking-axis optical conductivity displays a number of sharp peaks below 2000 cm^{-1} [Fig. 4(a)], attributed to the e-mv. It is known that for TTF-based donors the bridge C=C bond has the largest e-mv coupling constant.[22] To discuss the e-mv effect in detail, we show in Fig. 7 the six (v_i^ρ) A_g modes polarized in the molecular plane [curve (a)] and six A_u modes found in the optical conductivity spectrum along the stack [curve (b)], both below 6 K. It is seen that the A_u modes of the 0 site are almost degenerate with the corresponding A_g counterparts. On the contrary, $v_\alpha^{+0.96}$ (A_u) and $v_\gamma^{+0.96}$ (A_u) are redshifted from the position of A_g components by -7 and -30 cm^{-1}, respectively [$v_\beta^{+0.96}(A_u)$ was too weak to be safely identified].

In order to understand the effect of the $2k_F$ BCDW-II electronic structure on the vibrational spectrum, we have calculated the A_g and A_u vibronic modes of the symmetric tetramer[19] introduced earlier, using vibronic adiabatic Mulliken theory.[23] Figure 8 shows the site-charge (ρ at $0a$ and $0b$) dependence of the frequencies of A_g (solid lines) and A_u (broken lines) vibronic modes of v_γ (taken as an example), and unperturbed (dotted lines) modes.[24] The effect of the intratetramer interactions is most significant when the charge separation is small. The shifts of the frequencies of A_u and A_g branches are large, and the higher mode is almost charge independent in a wide range of the site charge. The deviation from the dashed straight line implies that the estimation of the site charge from the frequency shift of the A_g vibronic bands is unreliable except the region of $\rho<0.1$ and $\rho>0.9$, if the e-mv coupling constant is large. For the $(EDO\text{-}TTF)_2X$ ($X=PF_6$ and AsF_6), the frequencies of the four modes are given at $\rho=0.04$ shown by the vertical line. This calculation explains the almost degenerate feature between the A_g and A_u modes of charge-poor site and the downshift of the A_u mode at the charge-rich site. We roughly estimated the coupling constants as $g_\alpha\sim0.04$, $g_\beta<0.01$, and $g_\gamma\sim0.08$ eV to reproduce the splitting between the A_g and A_u modes at the charge-rich site. The downshift at charge-rich sites comes from the localized 11 pair at sites $1a$ and $1b$.

IV. CONCLUSION

In conclusion, we measured electronic and vibrational spectra of $(EDO\text{-}TTF)_2X$ ($X=PF_6$ and AsF_6). Our analysis shows the following things.

(1) The high-temperature metallic phase of $(EDO\text{-}TTF)_2X$ ($X=PF_6$ and AsF_6) can be described as a Q1D weak $4k_F$ BOW with a homogeneous (+0.5) charge on each site. The broad width of the Raman bands suggest a nearly localized nature of charge. The e-mv interaction along the stack is evident.

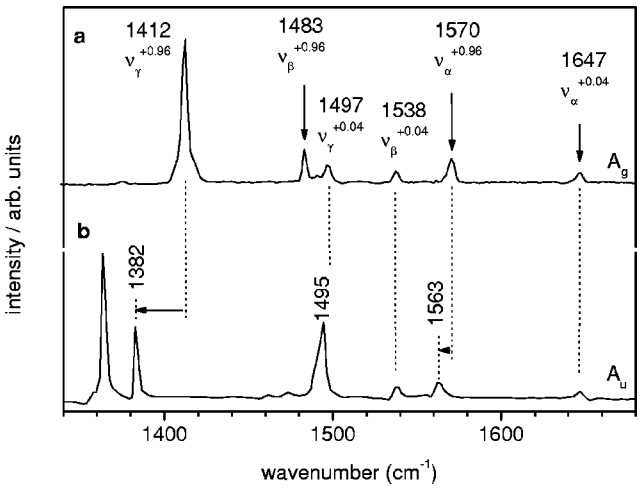

FIG. 7. v_i^ρ modes of $(EDO\text{-}TTF)_2AsF_6$ below 6 K: (a) A_g modes in the Raman spectra and (b) A_u modes in the optical conductivity spectrum for $E\|$stack. Arrows show softening of the A_u modes due to the e-mv coupling.

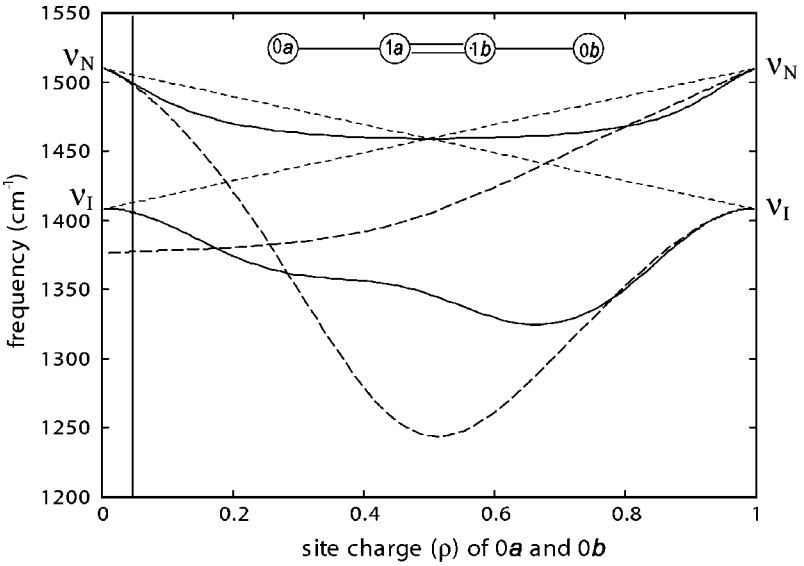

FIG. 8. Site-charge [ρ at $0a$ and $0b$ and $(1-\rho)$ at $1a$ and $1b$] dependence of $2A_g$ (charge-rich and charge-poor branches plotted by two solid lines) and $2A_u$ (charge-rich and charge-poor branches drawn by two broken lines) vibronic modes and unperturbed (dotted lines) modes in a symmetric tetramer with $t=0.15$, $t_1=0.28$, $\Delta=0.24$, $U=0.93$, and $g=0.08$ eV. v_N and v_I represent the frequencies of neutral and cationic molecules, respectively.

(2) The low-temperature insulating phase is a $2k_F$ BCDW-II with the large site charge difference ($2\delta\sim 0.9$) and a large bond order amplitude. Because the charge density is localized on the central 11 pair, the electronic spectra manifest a strong CT_2 band (mainly $|0110\rangle\rightarrow|0200\rangle$) and the $v_\alpha^{+0.96}$ and $v_\gamma^{+0.96}$ intramolecular C═C vibrations are strongly coupled to CT_2.

(3) It is generally agreed that 0110 periodicity requires a large U to prevent the double occupancy, and a sufficiently small V to allow two neighboring occupied sites. Most calculations devoted to this problem examine the $2k_F$ BCDW-I while no study up to date was able to reproduce the $2k_F$ BCDW-II with such a large charge and bond order in the framework of the purely electronic extended Hubbard model (except when next-neighbor V_2, etc., are included). It is clear that in organic CTS the individual properties of the molecule constituting a "site" should not be neglected. This includes the flexibility of EDO-TTF in the studied complexes, which serves as a means of interchange of two processes: variation of the site charge leading to the molecular deformation (and vice versa), and adjustment of the overlap integrals to the molecular geometry. To include such kind of interplay betwee the molecular charge, molecular deformation, and intermolecular π-π overlap, both the Peierls-type[7] and Holstein-type[25] electron-phonon interactions should be included in the extended Hubbard model in the future studies.

*Author to whom correspondence should be addressed. Electronic address: olga@ims.ac.jp

[1] D. S. Chow, F. Zamborsky, B. Alavi, D. J. Tantillo, A. Baur, C. A. Merlic, and S. E. Brown, Phys. Rev. Lett. **85**, 1698 (2000); F. Nad, P. Monceau, C. Carcel, and J. M. Fabre, Phys. Rev. B **62**, 1753 (2000); Y. Nogami, K. Oshima, K. Hiraki, and K. Kanoda, J. Phys. IV **9 Pr10**, 357 (1999).

[2] Y. Shibata, S. Nishimoto, and Y. Ohta, Phys. Rev. B **64**, 235107 (2001); M. Calandra, J. Merino, and R. H. McKenzie, *ibid.* **66**, 195102 (2002); H. Seo, J. Phys. Soc. Jpn. **69**, 805 (2000).

[3] J.-P. Pouget, J. Phys. IV **10**, 43 (2000).

[4] T. Mori, Bull. Chem. Soc. Jpn. **73**, 2243 (2000).

[5] J. Merino and R. H. McKenzie, Phys. Rev. Lett. **87**, 237002 (2001); S. Mazumdar, R. T. Clay, and D. K. Campbell, Phys. Rev. B **62**, 13 400 (2000).

[6] S. Mazumdar, S. Ramasesha, R. T. Clay, and D. K. Campbell, Phys. Rev. Lett. **82**, 1522 (1999).

[7] R. T. Clay, S. Mazumdar, and D. K. Campbell, Phys. Rev. B **67**, 115121 (2003).

[8] K. C. Ung, S. Mazumdar, and D. Toussaint, Phys. Rev. Lett. **73**, 2603 (1994).

[9] A. Ota, H. Yamochi, and G. Saito, J. Mater. Chem. **12**, 2600 (2002).

[10] O. Drozdova, K. Yakushi, A. Ota, H. Yamochi, and G. Saito, Synth. Met. **133–134**, 277 (2003).

[11] T. Ishiguro, K. Yamaji, and G. Saito, *Organic Superconductors* 2nd ed. (Springer, Berlin, 1998), p. 53.

[12] K. Yamamoto, K. Yakushi, K. Miyagawa, K. Kanoda, and A. Kawamoto, Phys. Rev. B **65**, 085110 (2002).

[13] O. Drozdova, H. Yamochi, K. Yakushi, M. Uruichi, S. Horiuchi, and G. Saito, J. Am. Chem. Soc. **122**, 4436 (2000).

[14] G. Saito, H. Sasaki, T. Aoki, Y. Yoshida, A. Otsuka, H. Yamochi, O. Drozdova, K. Yakushi, H. Kitagawa, and T. Mitani, J. Mater. Chem. **12**, 1640 (2002).

[15] The splitting of v_β of EDO-TTF^0 is attributed to the Fermi resonance probably with the overtone modes of the infrared-active C-S stretching at 774 cm^{-1}. The very similar splitting is found in $(BEDT\text{-}TTF)_2RbZn(SCN)_4$ (Ref. 12).

[16] H. S. Gutowsky and K. Sakai, J. Chem. Phys. **25**, 1228 (1953).

[17] J. Favand and F. Mila, Phys. Rev. B **54**, 10 425 (1996).

[18] X. Zotos, P. Prelovsek, and I. Sega, Phys. Rev. B **42**, 8445 (1990).

[19] V. M. Yartsev, Phys. Status Solidi B **125**, 501 (1984).

[20] K. D. Cummings, D. B. Tanner, and J. S. Miller, Phys. Rev. B **24**, 4142 (1981).

[21] The modes with the same symmetry at the charge-rich and charge-poor sites are slightly mixed with each other.
[22] G. Visentini, M. Sasino, C. Bellito, and A. Girlando, Phys. Rev. B **58**, 9460 (1998).
[23] A. Painelli and A. Girlando, J. Chem. Phys. **84**, 5655 (1986); K. Suzuki, K. Yamamoto, and K. Yakushi, Phys. Rev. B **69**, 085114 (2004).
[24] We changed the site energy difference to control the site charge from 0 to 1. The unperturbed frequency was assumed as $v_1(\rho) = v_{N\rho} + v_r(1-\rho)$ and $v_2(\rho) = v_N(1-\rho) + v_1\rho$, where v_N and v_I are the frequencies in neutral and ionic molecules, respectively.
[25] P. Maurel and M.-B. Lepetit, Phys. Rev. B **66**, 075117 (2002).